In-Situ Monitoring of Bottom-Up Percussion Drilling of Alkali-Free Alumina-Borosilicate Thin Glasses Using Single and Double Femtosecond Laser Pulses

John Lopez [*1], Samba Niane [2], Guillaume Bonamis [3], Pierre Balage [1], and Inka-Manek-Hönninger [1]

[1] *University of Bordeaux-CNRS-CEA, CELIA UMR5107, 33400 Talence, France*
[2] *ALPhANOV, rue François Mitterrand, 33400 Talence, France*
[3] *AMPLITUDE, 11 avenue de Canteranne, 33600 Pessac, France*
[*] *Corresponding author's e-mail : john.lopez@u-bordeaux.fr*

We report on top-down and bottom-up percussion drilling of alkali-free alumina-borosilicate glass using single and double femtosecond laser pulses. The drilling process dynamics are studied by pump-probe shadowgraphy under Brewster angle which allows for visualizing transient effects in the 300-µm thick glass. We show that the top-down drilling is very limited and does not allow for drilling through holes in contrast to the bottom-up approach. We study the influence of the laser parameters such as the fluence and focusing conditions which reveal to constitute key parameters in order to find an adequate process window for successful bottom-up drilling. We observe that the vertical velocity for bottom-up processing should be ideally in agreement with the ablation moving interface velocity. Interestingly, the shadowgraphs reveal that the drilling process may be interrupted even before any frontside ablation appears if the vertical velocity shift is too high. Moreover, we investigate the effects of introducing an additional spatial and temporal shift during the drilling process which lead to a significant increase in drilling rate by almost a factor of two.
DOI: 10.2961/jlmn.2022.01.2008
Keywords: laser drilling, top-down, bottom-up, glass, pump-probe

1. Introduction

Thin glass is widely used in modern manufacturing, especially in consumer electronics and flat display panel industries. Glasses are brittle and very sensitive to high thermal gradient, so that they require specific care to be processed. Ultrafast laser technology, which has the unique capacity to produce either surface ablation, bulk modification or backside ablation, is already used for glass processing [1]. However, combining good quality and high throughput is still a key issue.

Laser-based glass drilling has been already widely reported in the scientific literature. Drilling processes are based on percussion using CO_2 laser [2-3], UV laser [4-5], Bessel beam [6], single-pulse [7-8] or GHz-burst ultrafast laser [9], on water assisted laser drilling [10] or even on laser assisted chemical etching [11]. Thanks to non-linear absorption the drilling can be done from frontside (top-down) [7] or from backside (bottom-up) [8, 12].

Compared to frontside ablation, backside ablation enables (i) to produce sharper rims featuring lower taper angles on deep ablation craters, (ii) to limit the effects of ablation plume and plasma shielding, and (iii) to minimize deposition of debris in the processed area during the interaction. Conversely to frontside ablation where the energy deposition occurs into the skin depth [13], backside ablation leads to in-volume energy deposition upstream the theoretical focus due to non-linear absorption [14-15]; consequently, backside ablation is more sensitive to pulse duration variations [14-16] and beam focusing by the effective numerical aperture. Furthermore, backside ablation requires high numerical apertures and low fluences to avoid ablation at the front surface which interferes with the drilling process [8]. From a practical point of view, the drilling speed is defined by the ablation front velocity in top-down drilling whereas it is fixed by the vertical velocity of the focus (Vz) in bottom-up drilling.

Furthermore, it has been shown that splitting the laser pulse into two or more sub-pulses enables one to reduce detrimental non-linear propagation effects and to relocalize the energy deposition nearby the focus point [17].

We report here on time-resolved pump-probe shadowgraphy [15,18-20] of both top-down and bottom-up percussion drilling of alkali-free alumina-borosilicate 300-µm thin glasses (Schott AF32 eco) using single and double femtosecond laser pulses. We used a probe under Brewster angle incidence in order to visualize the transient bulk modification during the laser drilling process of the thin glass. The influence of numerical aperture, focus position, fluence, and vertical velocity (Vz, for bottom-up only) were investigated. We also compared single- to double-pulse laser irradiation, with and without spatial and temporal shifts for double-pulse laser irradiation. The results are discussed in terms of drilling rate and hole morphology.

2. Experimental

We used a commercial Yb-doped femtosecond laser system (Tangor, Amplitude) emitting at 1030 nm. The pulse duration is 500 fs. The maximum average power is 100 W. The repetition rate can be set from 1 Hz to 2 MHz thanks to an external acousto-optic modulator.

The experimental setup, depicted in Fig.1, includes a halfwave plate combined with a polarizer cube, a first par-

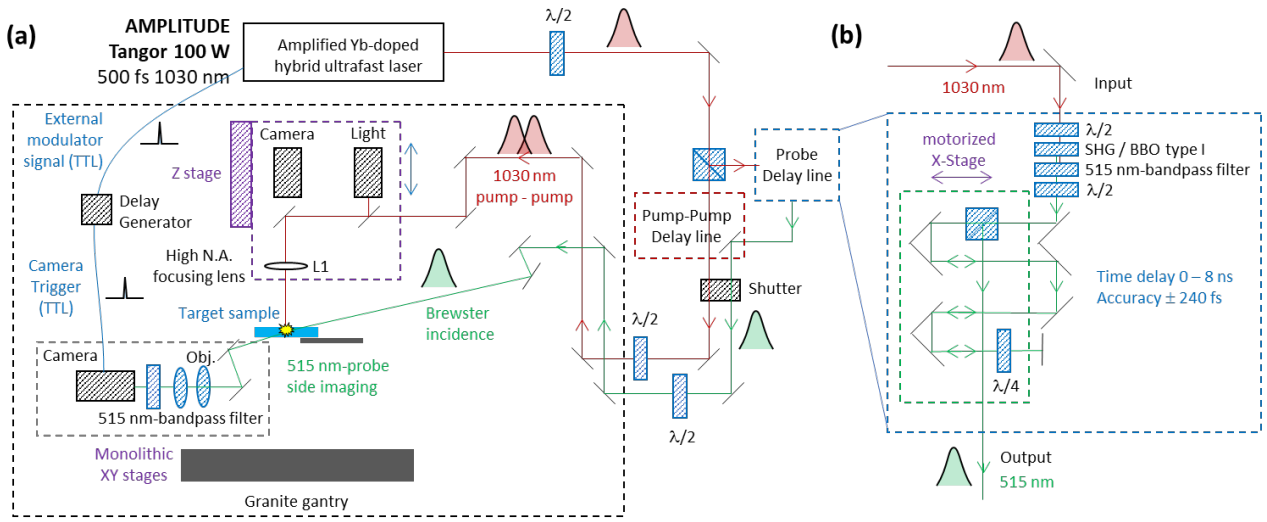

Fig. 1 Experimental setup used for top-down and bottom-up percussion drilling in glass (a), and delay line for the probe (b).

allel delay line for the probe, a second delay line for the double-pulse generation (pump-pump), a focusing head mounted on a Z-motorized axis (Alio Industries, AI-LM-10000-I-PLT-LP) and a focusing objective, which is either a 40-mm (Mitutoyo, model APO NIR x5/NA 0.14) or a 20-mm focal length objective (Mitutoyo, model APO NIR x10/NA 0.26). The Z-axis is used for focus setting and for moving upward the sample during bottom-up drilling. Then the target sample is placed on a 2-axes goniometer stage for flatness setting, which is mounted on a set of XY-motorized stages (Alio Industries, AI-LM-20000-XY-I-LP) for positioning the sample under the laser beam.

We measured the spot diameter at $1/e^2$ using a CDD camera (WinCamD LCM4) and a homemade magnification system calibrated with a standard micro rule (Mitutoyo, model 375-056). Table 1 presents the beam size (before focus), the effective numerical aperture, the spot diameter and the Rayleigh length for the two focusing configurations (20-mm or 40-mm focusing objective). The spot diameter was 7.3 µm with the 40-mm objective and 3.7 µm with the 20-mm objective resulting in maximum fluences of 150 J/cm² and 510 J/cm², respectively. The repetition rate was set to 5 Hz for all drilling experiments.

Table 1 Beam size before focus, focal length, numerical aperture, spot diameter and Rayleigh length for the two focusing configurations

Material	Obj. x5	Obj. 10x
Beam size (mm)	10.7	10.4
Focal length (mm)	40	20
Numerical aperture	0.13	0.25
Spot diameter (µm)	7.3	3.7
Rayleigh length (µm)	~45	~8

2.1 Pump-pump setup for double pulse irradiation

The double pulse at 1030 nm is generated owing to a pump-pump optical delay line where the initial pulse from the laser output is split into two sub-pulses with a controlled time delay. This delay line has been already described in detail in previous papers [13,21]. Each arm has its own halfwave plate and polarizer cube allowing for adjusting the sub-pulse energies independently of each other in the two arms. The energy ratio between the two arms is set to 100:0 for single pulse irradiation and to 50:50 for double pulse irradiation. Moreover, each arm has its own variable beam expander in order to set the focus at the same location and the spot diameter at the same value for the two arms; However, it is possible to introduce a vertical (Δz) or a temporal shift (Δt) on purpose between the two sub-pulses by adjusting the beam collimation and the optical path on one arm. The polarization of the two sub-pulses is linear at the output of the pump-pump delay line.

2.2 Pump-probe setup for time-resolved shadowgraphy

The 1030-nm incoming laser pulse is frequency doubled using a type I BBO crystal, then filtered with a 515-nm bandpass filter and delayed owing to a motorized delay line. The optical path variation is up to 2.4 m corresponding to a 0 – 8 ns time delay. The probe laser beam is transmitted through the sample under Brewster incidence and then straightened horizontally to be directed towards the sensor. The probe signal is then collected by a long-distance microscope (InfiniMax KX, with MX-5 objective), followed by a second zoom objective (InfiniMax, x2 ring) and two 515-nm bandpass filters, and then imaged on a CMOS camera (Basler acA1920-25mu, resolution of 1920 × 1080p, pixel size 2.2 µm x 2.2 µm, 25 fps, rolling shutter). Conversely to transverse probing [7-9,15,18-20] which leads to a blurred zone around both the front and rear surfaces (Fig. 2a), probing under Brewster incidence enables to observe bulk modifications along the glass thickness without any shadow effect due to the sample edges, even for thin or ultrathin glass samples (Fig. 2b). The side camera is triggered by a TTL signal from the acousto-optic modulator at the exit of the laser source which is filtered and optionally delayed by an electronic generator (Tombak, Aerodiode). In practice, we focus the pump laser beam onto the front surface in order to produce an ablation crater for each single pulse. The trigger signal generated by probe pulse N allows for imaging the ablation crater induced by pump pulse N+1, whereas the ablation crater of pump pulse N remains visible. We define the zero delay as the onset of surface modification after the pump pulse N+1. The temporal resolution is determined by the probe pulse duration

(500 fs) and the precision in the path delay of the probe delay line, which is 80 µm and corresponds to 264 fs. The recording time between two subsequent image captures is limited by the acquisition time of the camera (40 ms) and the buffer refreshing time (160 ms), and thus restricted to 200 ms. Therefore, all pump-probe and drilling experiments were performed at low repetition rate (5 Hz) in order to be able to get one capture after each laser pulse.

In a preliminary study dedicated to front surface ablation, we varied the probe delay to determine the delay giving the most visible transient modification**.** Therefore, the probe delay was set to 4.4 ns for percussion drilling experiments in single pulse mode, and to 4.4 ns with respect to the first sub-pulse for percussion drilling experiments in double pulse mode.

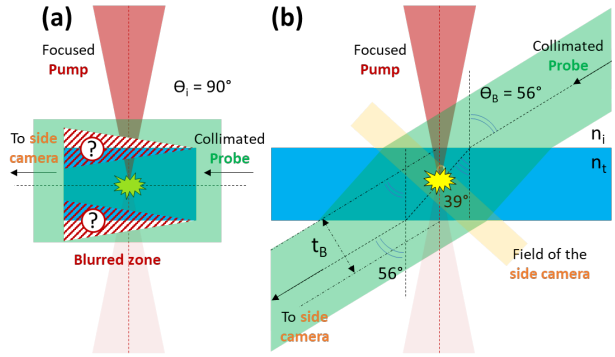

Fig. 2 Schematic view of the pump and the probe incidences on the glass sample with a transverse probe (a) or with a probe under Brewster incidence (b). Θ_B is the Brewster angle (56°), t_G is the glass thickness (300 µm) and t_B is the apparent glass thickness under Brewster incidence (249 µm). The scale factor of the Z-axis is t_B/t_G = 0.83 in (b).

From a practical point of view, we recorded one picture every ten pulses in order to limit the data volume. The hole depths were measured from pump-probe captures using ImageJ open access software. The drilling rate, in µm per pulse, is defined as the slope (linear fit) of the hole depth versus pulse number curve. The drilling speed, in µm per second, is the drilling rate multiplied by the repetition rate. The uncertainty is (-9/+0) on the pulse number for the onset of upward drilling and there is no uncertainty for all following pulse numbers (+10 pulses for consecutive images). The uncertainty on the drilling rate is about ± 0.02 µm per pulse.

Finally, the Brewster angle Θ_B value is given by the following formula:

$$\Theta_B = Arctan\,(n_t / n_i) \qquad (1)$$

where n_t and n_i are the refractive index of glass and air respectively. The Brewster angle value is 56° for AF32 glass, and therefore, the probe beam incidence is set at 56° with respect to normal incidence (Fig. 2). Within the sample, the probe beam incidence drops to 39° due to optical refraction, and then returns to 56° after the glass.

The apparent thickness of the glass sheet t_B viewed by the camera under Brewster incidence is given by the following formula:

$$t_B = t_G \cdot sin(\Theta_B) \qquad (2)$$

where t_G is the glass thickness. Note that captures obtained under Brewster angle suffer from a deformation on the Z-axis only (Fig. 2). The apparent glass thickness is smaller than the real one; the scale factor is given by the ratio t_B/t_G = 0.83. For the same reason, the holes observed under Brewster incidence will appear smaller in Z than they are in reality.

2.3 Numerical aperture

As explained previously, the numerical aperture and the fluence are two key parameters for backside ablation and bottom-up drilling. Indeed, a high numerical aperture and a low fluence contribute to avoid frontside ablation - which induces detrimental energy losses and beam propagation distortion upstream the focal plane - and enable to achieve selective backside ablation [8]. This is even more true for thin glass as well as at the end of the bottom-up drilling process where the remaining glass thickness is small.

Fig. 3 and Fig. 4 present the fluence process windows for the two focusing configurations, i.e., 40-mm and 20-mm focusing objective, respectively. The principle of this experiment is to deliver a 50-pulses train at 5 Hz at different Z locations on either side of the glass for different fluences. The red crosses symbolize that frontside ablation occurs after 50 pulses at the aimed Z location, whereas the green crosses indicate that backside ablation occurs after 50 pulses at the aimed Z location. This experiment shows that it is impossible to perform backside ablation without damaging the front surface for fluences above 70 J/cm² with the 40-mm focusing objective (Fig. 3). The longer focal lens is not suitable for backside ablation since frontside ablation occurs already when the focus is set at mid-thickness at a fluence of only 10 J/cm² (Fig. 3). Conversely to the longer focal length, the shorter focal length enables selective backside ablation at 28 J/cm² (Fig. 4). Once the ablation happens at the rear side, the surface roughness in the ablation crater will improve the energy deposition leading to bottom-up drilling. Therefore, the 20-mm focusing objective could be used for bottom-up drilling.

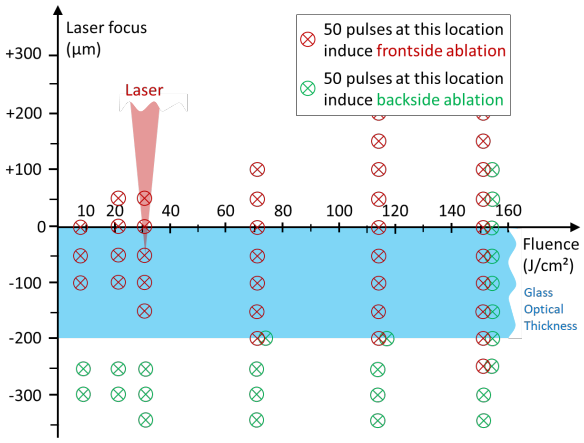

Fig. 3 Frontside and backside ablation appearance after a 50-pulses train at different Z locations on either side of the glass, for fluences ranging from 8 to 150 J/cm² with the 40-mm focusing lens. The repetition rate is 5 Hz.

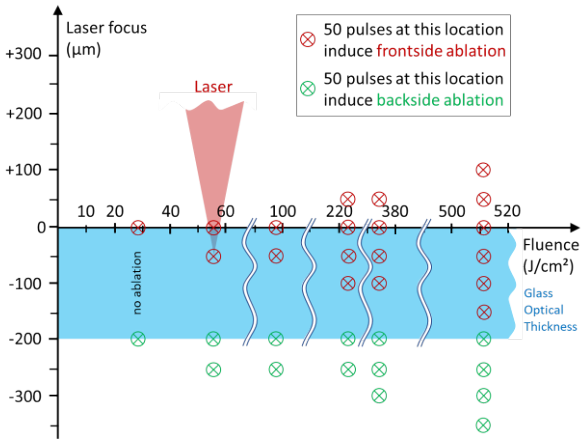

Fig. 4 Frontside and backside ablation appearance after a 50-pulses train at different Z locations on either side of the glass, for fluences ranging from 28 to 510 J/cm² with the 20-mm focusing lens. The repetition rate is 5 Hz.

2.4 Target material

All drilling experiments were performed on a 300-µm thick alkali-free alumina-borosilicate glass (Schott AF32 eco). This glass has a thermal expansion coefficient of $3.2 \cdot 10^{-6}$ K^{-1} within the range 20 – 300 °C [22], which is similar to silicon, so it is ideally suitable to wafer-level packaging in the semiconductor industry or in MEMS devices. The refractive index is 1.51, so the optical thickness of the sample is about 199 µm.

3. Top-down percussion drilling

Single pulse top-down percussion drilling is mainly performed with the 40-mm focusing lens in order to maximize the focus depth and the spot diameter (compared to the 20-mm focusing lens). The focus is set onto the front surface of the glass. The repetition rate is set to 5 Hz for pump-probe imaging during the drilling process.

Fig. 5 presents permanent modifications after top-down percussion drilling in single-pulse mode for different drilling times, focus position and incident fluences. Fig. 5a illustrates that the hole depth does not increase when the drilling time rises from 60 to 80 sec. Note that the scalebar in Fig. 5 corresponds to the Z axis only. Furthermore, Fig. 5b indicates that the hole depth does not improve even if the focus is set inside the glass sheet. Finally, Fig. 5c shows that increasing the fluence from 49 to 493 J/cm² is insufficient to go through the thin glass sheet even after an 80-s drilling time (the depth increases by a factor of 4 whereas the fluence increases by a factor of 10). The drilling speed is about 1.5 µm per second, so the drilling rate is about 0.3 µm per pulse at 493 J/cm² (120 µm ablated in 400 pulses). These results highlight the limitation in top-down percussion drilling; the holes are short, blind, and highly tapered. The drilling is over after few hundred of pulses.

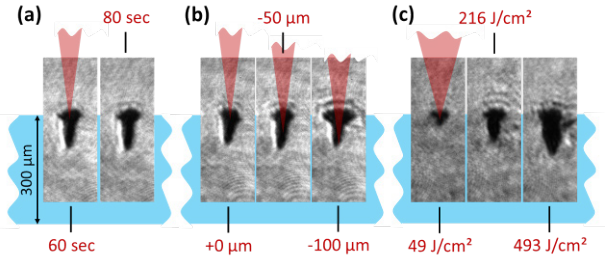

Fig. 5 Permanent modification after single pulse top-down percussion drilling. The changing parameter is the drilling time for (a), the focus position for (b) and the fluence for (c). The repetition rate is 5 Hz. The focal length is 40 mm for (a) and (b), whereas it is 20 mm for (c). The fluence is 74.5 J/cm² for (a) and (b). Drilling time is 70 sec for (b) and 80 sec for (c). The blue area materializes the glass thickness.

4. Bottom-up percussion drilling

As mentioned in the introduction section, bottom-up percussion drilling brings several advantages compared to top-down processing. Indeed, the laser beam propagates directly to the tip of the forming hole leading to sharp rims and low taper inner walls. Furthermore, the drilling process is less sensitive to plume or debris shielding. However, the crucial point is to avoid frontside ablation otherwise the drilling process is over. Conversely to [8], our strategy for bottom-up drilling is to use a short focal length and an upward moving focus. Thus, the drilling speed is imposed by the vertical velocity of the focus (Vz) which is ideally set to be similar to the ablation moving interface velocity (Vi). If Vz > Vi, then the drilling process drops out leading to a blind hole; on the contrary, if Vz < Vi, then the process is inefficient and debris recast is possible.

As in [8], the starting focus point is set 50 µm below the rear surface in order to make coincide the rear surface and the highest energy deposition region [15,23], which depends on the pulse duration, the fluence and the numerical aperture. Note that the energy deposition occurs in a large volume in the converging beam upstream the focus point. Therefore, the calculated fluence is a theoretical value which is never reached at the rear surface [8,14,22].

We used the 20-mm focusing objective for all bottom-up drilling experiments, and the repetition rate was 5 Hz.

Fig. 6a and 7a show time-resolved shadowgraphs of bottom-up percussion drilling for 56 J/cm² and 218 J/cm², respectively. The vertical velocity (Vz) was set to 1 µm/s to coincide with the estimated drilling speed. The probe beam delay was chosen to 4.4 ns as for this value the transient bulk modifications are clearly visible. Fig. 6b and 7b present the corresponding hole depths as a function of pulse number. At 56 J/cm², we observe a blind hole at the rear surface and an ablation crater at the front one. The upward drilling rate is 0.16 µm per pulse, so the drilling speed is 0.80 µm per second. We note that the drilling process drops out before any crater appearance onto the front surface. This point is especially visible on Fig. 6 where the crater appears clearly after the bottom-up drilling has already stopped. At 218 J/cm² (Fig. 7), the higher fluence contributes to enlarge the hole and to make the junction between the upward forming hole and the downward ablation crater.

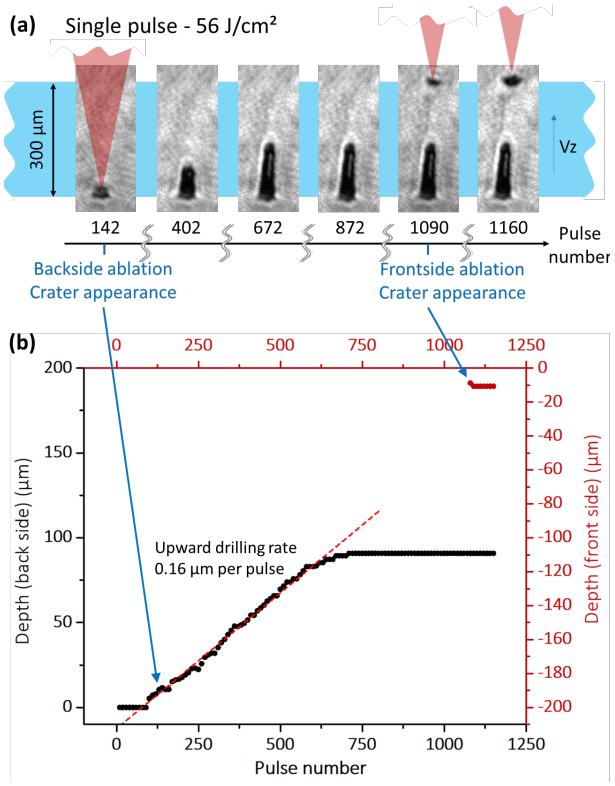

Fig. 6 Pump-probe imaging captures for pulse numbers ranging from 142 to 1160 (a) and hole depth versus pulse number (b) during bottom-up percussion drilling in a 300-µm thick AF32 glass sheet using single femtosecond pulse irradiation. The incident pulse fluence is 56 J/cm². The vertical velocity (Vz) is 1 µm/s. The pulse number axis in (a) is not to scale. The onset of upward drilling appears after 72 pulses. Below this latter value the main energy deposition location is under the rear surface. The extracted drilling rate from the slope measurement in (b) is 0.16 µm per pulse, so the drilling speed is 0.80 µm per second at 5 Hz.

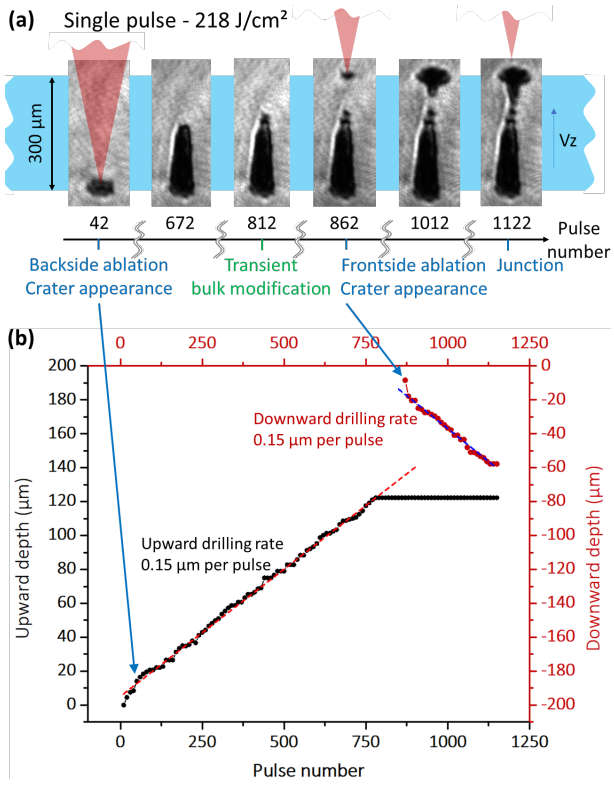

Fig. 7 Pump-probe imaging captures for pulse numbers ranging from 42 to 1122 (a) and hole depth versus pulse number (b) during bottom-up percussion drilling in a 300-µm thick AF32 glass sheet using single femtosecond pulse irradiation. The incident pulse fluences is 218 J/cm². The vertical velocity (Vz) is 1 µm/s. The pulse number axis in (a) is not to scale. The onset of upward drilling appears after 2 pulses only due to high fluence. The extracted drilling rate from the slope measurement in (b) is 0.15 µm per pulse, so the drilling speed is 0.75 µm per second at 5 Hz.

More interestingly, we observe that the ablation switches from the rear to the front surface as the hole goes upward and gets closer to the front surface; then the downward forming hole will create the junction. This phenomenon was already observed during bottom-up trepanning drilling of sapphire [24]. Both the upward and the downward drilling rates are 0.15 µm per pulse. Therefore, there is no beneficial effect, neither on the drilling rate nor the drilling speed, while increasing the fluence from 56 to 218 J/cm². The hole goes through, but its shape is uneven. The junction zone appears as a bottleneck encumbered with some debris.

Fig. 8a presents the permanent modification obtained after bottom-up drilling at 1 µm/s (Vz) for different fluences ranging from 56 to 358 J/cm². For the highest fluence value of 358 J/cm², the ablation switches to the front surface at an early stage of the drilling process (Fig. 8a). The ablation crater is wide and penetrates only on the first third of the glass thickness; obviously, high fluence is counterproductive.

We performed the same experiment in the double-pulse configuration (Fig. 8b). As for the single-pulse study, the vertical velocity is 1 µm/s and the total incident fluence is 56 J/cm² (2 x 28 J/cm²). We observe that the drilling process stops at mid-thickness like in the single-pulse case (Fig. 8a, left).

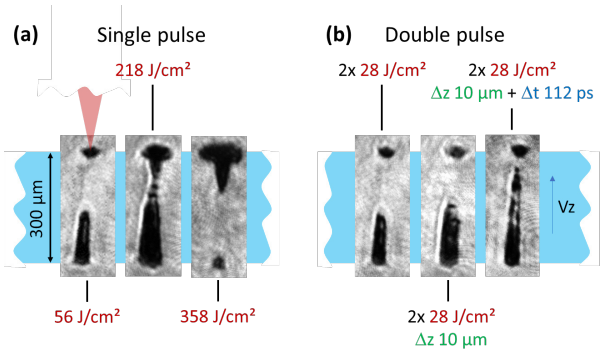

Fig. 8 Permanent modification after bottom-up percussion drilling, (a) for single pulse irradiation at different fluence values, and (b) for double-pulse irradiation without (left), with spatial shift (middle), and with spatial and temporal shifts (right). The vertical velocity (Vz) is 1 µm/s. The drilling starts at 50 µm below the rear surface.

Fig. 9a and 10a display the pump-probe imaging captures of bottom-up percussion drilling in double-pulse configuration, without and with temporal Δt and spatial shift Δz, respectively. Fig. 9b and 10b present the corresponding hole depth as a function of pulse number. Regarding Fig. 8 and 9, we note that splitting the incoming pulse into two sub-pulses aiming at the same location at the same time (no temporal shift, no spatial shift) does not lead to any improvement, neither on the upward drilling rate (0.16 µm per pulse, derived from Fig. 9b) nor on the hole depth.

Furthermore, we introduced a 10-µm spatial shift (Δz) between the two sub-pulses (Fig. 8b, middle). The second sub-pulse is now focused 10 µm upstream the first one. We measured a 20-% longer hole and a constant drilling rate (0.16 µm per pulse, not shown here) with respect to the single pulse approach. This beneficial effect on the hole depth could be explained by the fact that the second pulse pre-damages the glass upstream the ablation front, like an incubation effect, so the subsequent double-pulse is more efficient for drilling. Note, if the spatial shift is only 3 µm, the hole depth drops down by 40% in comparison to single pulse drilling (result not shown in Fig. 8b for sake of conciseness). This could be explained by the fact that the second sub-pulse arrives within the volume which is already in interaction with the first sub-pulse. So, the influence of a spatial shift depends on its value, it can be beneficial, or counter-productive when the shift is too low.

Finally, if the second pulse is additionally delayed by Δt = 112 ps, conserving the spatial delay of Δz = 10 µm, we observe a longer hole (x 1.7) with respect to the single pulse regime (Fig. 8). Based on this result, we adapted the vertical velocity to 1.7 µm/s and observe an increase of the drilling rate to 0.31 µm per pulse (Fig. 10b). The time delay Δt, exceeding 100 ps, was chosen on purpose to ensure that the energy deposition of the second sub-pulse takes place after the matter removal and shockwave emission induced by the first sub-pulse [1]. Nevertheless, this delay value is short enough to avoid any thermal diffusion in the lattice. We observe that the bottom-up drilling process stops just below the front surface. We assume that the long temporal shift permits to reduce efficiently transient detrimental shielding effects. However, the hole does not go through either.

Furthermore, comparing the double pulse shadowgraphs to the single-pulse case (Fig. 6) we clearly observe a transient effect moving upward, which is intensified by the additional temporal and spatial shifts (Fig. 10). We assume that dividing the pulse into two sub-pulses contributes to reduce the non-linear effects along the beam propagation, to relocalize the energy deposition nearby the focus point and consequently to enhance the free-electron density in the conductive band.

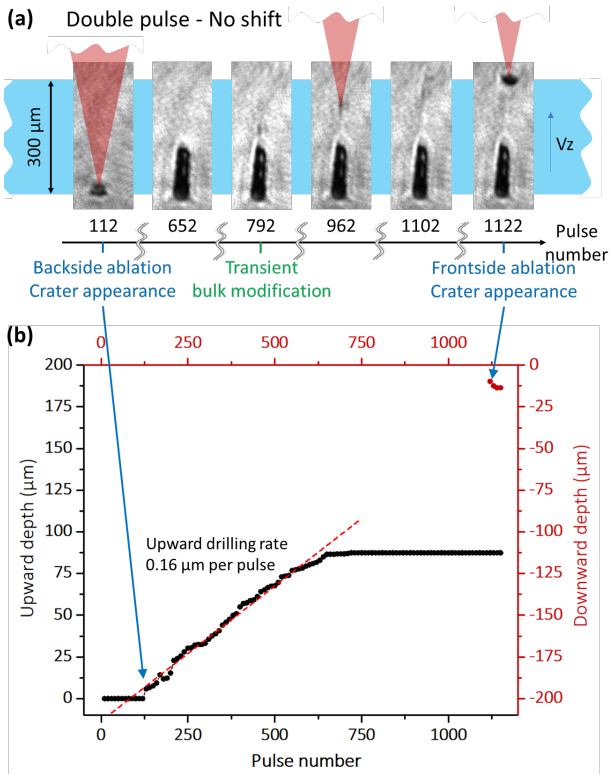

Fig. 9 Pump-probe imaging capture for pulse numbers ranging from 112 to 1122 (a) and hole depth versus pulse number (b) during bottom-up percussion drilling in a 300-µm thick AF32 glass sheet using double femtosecond pulse irradiation without any temporal nor spatial shift. The sub-pulse fluence is 28 J/cm², corresponding to a total fluence of 56 J/cm². The vertical velocity (Vz) is 1.0 µm/s. The pulse number axis in (a) is not to scale. The onset of upward drilling appears after 112 pulses. The extracted drilling rate from the slope measurement in (b) is 0.16 µm per pulse, so the drilling speed is 0.80 µm per second at 5 Hz.

In order to understand why the drilling process stops we tried different vertical velocities (Vz) ranging from 0.5 to 2.0 µm/s; the obtained permanent modifications are depicted in Fig. 11. If the velocity is too high, there is no benefit. The drilling process stops half-way. On the contrary, if the velocity is too slow, the hole length increases significantly. The hole becomes tapered, and some debris aggregate inside the hole, as it is observed for 0.5 and 1 µm/s. The hole does not go through even if the vertical velocity is lower than the measured drilling speed. Indeed, the drilling process stops 20 µm below the front surface at 1 µm/s. It is possible to go through at 0.5 µm/s, but the second half of the hole is fully encumbered with debris. Therefore, the key point seems to be the debris draining outside the hole. Water assisted laser drilling [10] could be a solution to remove the ablation debris from the forming hole.

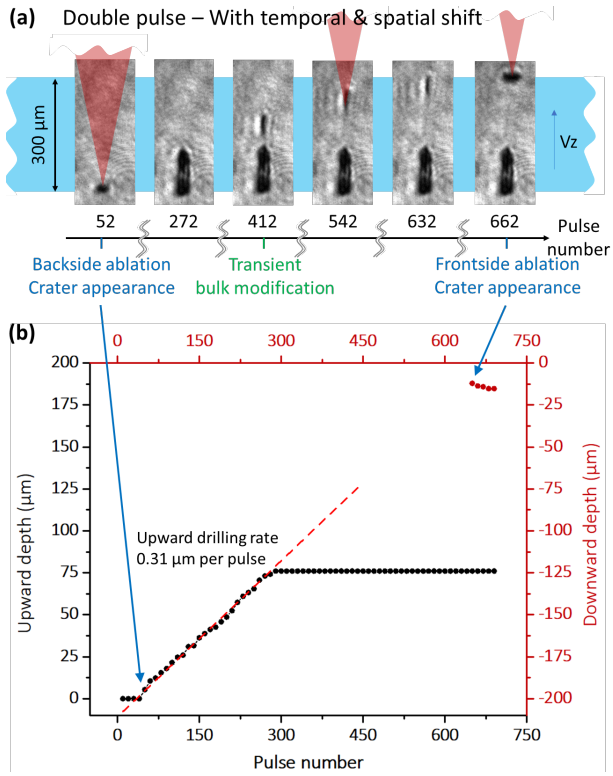

Fig. 10 Pump-probe imaging capture for pulse numbers ranging from 52 to 662 (a) and hole depth versus pulse number (b) during bottom-up percussion drilling in a 300-µm thick AF32 glass sheet using double femtosecond pulse irradiation. The temporal and spatial shifts between the two subsequent sub-pulses are 112 ps and 10 µm, respectively. The sub-pulse fluence is 28 J/cm², corresponding to a total fluence of 56 J/cm². The vertical velocity (Vz) is 1.7 µm/s. The pulse number axis in (a) is not to scale. The onset of upward drilling appears after 42 pulses. The extracted drilling rate from the slope measurement in (b) is 0.31 µm per pulse, so the drilling speed is 1.55 µm per second at 5 Hz.

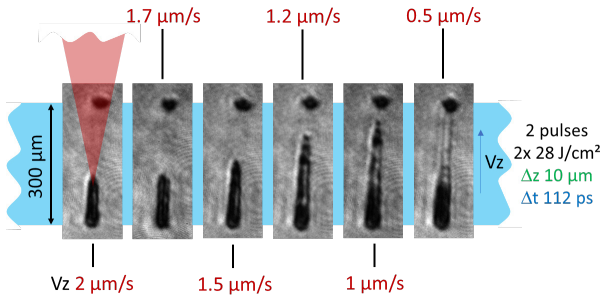

Fig. 11 Permanent modification after double femtosecond pulses drilling for different vertical velocities (Vz) ranging from 0.5 to 2 µm/s. The temporal shift (Δt, blue) is 112 ps whereas the spatial shift (Δz, green) is 10 µm between the two subsequent sub-pulses. The incident sub-pulse fluence is 28 J/cm².

5. Conclusion

Top-down and bottom-up percussion drilling of 300-µm thick AF32 glass using single and double femtosecond laser pulses was investigated using pump-probe shadowgraphy. We used a probe beam under Brewster angle incidence in order to visualize the transient bulk modification during the laser drilling process of the thin glass. The holes obtained with the top-down process are short, blind, and highly tapered even at high fluence; the drilling is interrupted after few hundred of pulses. The bottom-up process is more convenient to produce thin and elongated holes; however, it is difficult to avoid the ablation switch from the rear side to the front side when the forming hole gets closer to the front surface. Both numerical aperture and incident fluence are key parameters for selective backside ablation. The vertical velocity for bottom-up processing should be ideally in agreement with the ablation moving interface velocity. The drilling process suffers from a dropout when the vertical velocity is too high, even before any frontside ablation crater appearance. Debris draining outside the forming hole appears to be another crucial point to go through. Finally, we also observed a significant improvement of drilling rate (from 0.16 to 0.31 µm per pulse) and aspect ratios by introducing a vertical (Δz) and temporal shift (Δt) between the two subsequent sub-pulses.

Acknowledgments

The authors thank the French *Ministère de l'Economie, des Finances et de l'Industrie* for support and funding (grant 172906051, 172906052 and 172906053).

References

[1] R.R. Gattass and E. Mazur: Nat. Photonics, 2, (2008) 219.
[2] H. Ogura and Y. Yoshida: Jpn. J. Appl. Phys., 42, (2003) 2881.
[3] L. Brusberg, M. Queisser, C. Gentsch, H. Schröder, and K.-D. Lang: Physics Procedia, 39, (2012) 548.
[4] H. Hidai, S. Matsusaka, A. Chiba, and N. Morita: Appl. Phys. A, 120 (2015) 357.
[5] Y. Kawasuji, J. Fujimoto, M. Kobayashi, A. Suwa, A. Mizutani, M. Arakawa, T. Onose, and H. Mizoguchi: J. Laser Appl., 32, (2020) 022076.
[6] F. Courvoisier, J. Zhang, M.K. Bhuyan, M. Jacquot, and J.M. Dudley: Appl. Phys. A, 112, (2013) 29.
[7] D. Grossmann, M. Reininghaus, C. Kalupka, M. Kumkar, and R. Poprawe: Opt. Express, 24, (2016) 23221.
[8] D. Grossmann, M. Reininghaus, C. Kalupka, M. Jenne, and M. Kumkar: Opt. Express, 25, (2017) 28478.
[9] J. Lopez, S. Niane, G. Bonamis, P. Balage, E. Audouard, C. Hönninger, E. Mottay, and I. Manek-Hönninger: Opt. Express, 30, (2022) 12533.
[10] R. An, Y. Li, Y. Dou, H. Yang, and Q. Gong: Opt. Express, 13, (2005) 1855.
[11] Y. Bellouard, A. Said, M. Dugan, and P. Bado: Opt. Express, 12, (2004) 2120.
[12] K. Mishchik, K. Gaudfrin, and J. Lopez: J. Laser Micro Nanoengin., 12, (2017) 321.
[13] K. Gaudfrin, J. Lopez, K. Mishchik, L. Gemini, R. Kling, and G. Duchateau: Opt. Express, 28, (2020) 15189.
[14] I.M. Burakov, N.M. Bulgakova, R. Stoian, A. Mermillod-Blondin, E. Audouard, and A. Rosenfeld: J. Appl. Phys., 101, (2007) 043506.

[15] M. Jenne, F. Zimmermann, D. Flamm, D. Groβmann, J. Kleiner, M. Kumkar, and S. Nolte: J. Laser Micro Nanoengin., 13, (2018) 273.
[16] P.K. Velpula, M.K. Bhuyan, C. Mauclair, J.P. Colombier, and R. Stoian: Opt. Eng., 53, (2014) 076108-1.
[17] K. Mishchik, R. Beuton, O. Dematteo, S. Skupin, B. Chimier, G. Duchateau, B. Chassagne, R. Kling, C. Honninger, E. Mottay, and J. Lopez: Opt. Express, 25, (2017) 33271.
[18] X. Mao, S.S. Sao, and R.E. Russo: Appl. Phys. Lett., 82, (2003) 697.
[19] S.S Mao, F. Quéré, S. Guizard, X. Mao, R.E. Russo, G. Petite and P. Martin: Appl. Phys. A, 79, (2004) 16895.
[20] Q. Sun, H. Jiang, Y. Liu, Z. Wu, H. Yang, and Q. Gong: Opt. Lett., 30, (2005) 320.
[21] K. Gaudfrin, G. Duchateau, K. Mishchik, R. Kling, and J. Lopez: Proc. SPIE, Vol. 10905, (2019) 109050H.
[22] Schott, "Electrical Properties of SCHOTT Thin Glasses", September 2018.
[23] O. Dematteo Caulier, K. Mishchik, B. Chimier, S. Skupin, A. Bourgeade, C. Javaux Léger, R. Kling, C. Hönninger, J. Lopez, V. Tikhonchuk, and G. Duchateau: Appl. Phys. Lett., 107, (2015) 181110.
[24] G. Lott, N. Falleto, P.-J. Devilder, and R. Kling: J. Laser Appl., 28, (2016) 022206.

(Received: June 2, 2022, Accepted: July 29, 2022)